Available online at www.sciencedirect.com
SCIENCE DIRECT®
International Journal of Heat and Mass Transfer 47 (2004) 1613–1625
International Journal of HEAT and MASS TRANSFER
www.elsevier.com/locate/ijhmt

Flow field of an unconfined low-Reynolds-number binary-mixture slot jet

An-Kuo Hsu [a], Jen-Yung Pu [a], Shuhn-Shyurng Hou [b], Ta-Hui Lin [a,*]

[a] Department of Mechanical Engineering, National Cheng Kung University, Tainan 70101, Taiwan, ROC
[b] Department of Mechanical Engineering, Kun Shan University of Technology, Tainan 71003, Taiwan, ROC

Received 2 May 2003; received in revised form 31 October 2003

Abstract

The flow field of a slot jet at low Reynolds numbers ($Re = 39.4$ and 78.8) was examined numerically and experimentally. The slot exit velocities are small, so the gravitational force has to be taken into consideration in numerical calculation. Experimentally, the fluid containing oxygen and nitrogen was issued from a slot jet into the quiescent atmosphere. The concentration field was measured by using a gas chromatograph and a gas-extracting quartz probe. Furthermore, smoke particles were used to visualize the flow field.

Due to the interaction among momentum transfer, mass transfer and gravitational force, the flow and concentration fields at low Reynolds numbers with considerable mass transfer are found very different from those at high Reynolds numbers. The flow field is greatly influenced by the gravitational force due to concentration-induced density change; and the flow field in turn affects the concentration distribution. For an upward jet of density higher than air, at $Re = 39.4$, one vortex in the far region exists. However, at $Re = 78.8$, two vortices appear; one attached at the slot exit and one in the far region. The calculated concentration field is in fairly good agreement with the experimental result.

Keywords: Low Reynolds number; Slot jet; Mass transfer; Concentration field; Gravitational force

1. Introduction

The slot jets have extensive applications in engineering and science in recent years. The study of slot jets can be classified by their boundary as confined (e.g. impinging jets for heating or drying) or as unconfined flow field (e.g. leakage of gas fuel from pipe into quiescent atmosphere). It can also be classified as high-Reynolds-number (e.g. turbulent jets) and as low-Reynolds-number flow fields (e.g. slit burners of domestic gas furnaces). Many researchers studied confined or semi-confined slot jets at high Reynolds numbers, and some researchers focused on the study of energy transfer for a flame of a slot jet burner.

Panzer and Telionis [1] used hot wire anemometry and flow visualization to examine the velocity distribution and cross-sectional shapes of jets issuing from slotted orifices. Their results indicated that for slots cut on thin tubes, the jets spread strongly in the transverse direction. Moreover, the jets appeared to have kidney-shaped cross-sections and double-peaked velocity distributions.

Baydar [2] experimentally investigated the flow field between two horizontal surfaces arising from flow issuing from a single jet or double jet on the lower surface and impinging normally on the upper surface. The velocity and pressure distributions in the impingement region were obtained over a Reynolds number range of 300–10 000 and a nozzle-to-plate spacing range of 0.5–4 slot widths. The effects of Reynolds number and nozzle-to-plate spacing on the flow structure were reported.

Roper et al. [3] described experiments to test the diffusion flame theory and found that the flame size can

* Corresponding author. Tel.: +886-6-2757575x62167; fax: +886-6-2352973.
E-mail address: thlin@mail.ncku.edu.tw (T.-H. Lin).

0017-9310/$ - see front matter © 2003 Elsevier Ltd. All rights reserved.
doi:10.1016/j.ijheatmasstransfer.2003.10.030

Nomenclature

Dimensional quantities

b'	width of the slot exit
$D'_{O_2-N_2}$	diffusivity between O_2 and N_2
g'	gravitational acceleration
P'	pressure in the flow field
u'	fluid velocity in x-direction
V'_{in}	slot exit velocity
v'	fluid velocity in y-direction
x'	transverse coordinate
y'	longitudinal coordinate
μ'_{mix}	absolute viscosity of the mixture
μ'_{O_2}	absolute viscosity of oxygen
ρ'	density of the fluid

Non-dimensional quantities

Fr	Froude number
P	non-dimensional pressure in the flow field
Re^*	Reynolds number
Sc^*	Schmidt number
S_ϕ	non-dimensional source term
x	non-dimensional transverse coordinate
y	non-dimensional longitudinal coordinate
Y_{N_2}	mole fraction of nitrogen in mixture
Y_{O_2}	non-dimensional mole fraction of oxygen in Eq. (2)
$Y_{O_2,in}$	mole fraction of oxygen at slot exit
$Y_{O_2,\infty}$	ambient oxygen concentration
μ_{mix}	non-dimensional absolute viscosity of the mixture, $\mu_{mix} = \mu'_{mix}/\mu'_{O_2}$
ρ	non-dimensional density of the fluid, $\rho = \rho'/\rho'_{O_2}$

be controlled either by momentum or by buoyancy effects for the slot burner.

Yuan et al. [4] proposed an experiment to simulate flame flickering comprising a free ascending column fed on its side with a light gas (helium) emerging from a vertical slot in ambient air.

Amielh et al. [5] studied experimentally the near-field region of variable density turbulent jets. The velocity measurements were performed using a two-component laser Doppler anemometer in an axisymmetric jet of helium, air or CO_2 exhausting into a low-speed air co-flow. The result indicated that the development of a lower density gas is more rapid than that of a heavier gas for either the same exit momentum flux or the same Reynolds number.

Mallens et al. [6] presented a model for laminar premixed Bunsen flames on slit burners burning in a surrounding atmosphere and investigated the influence of a surrounding atmosphere and burner curvature on the flame shape, flow field and mass transport in 2D laminar premixed Bunsen flames.

Lin et al. [7] performed an experimental study on heat transfer behavior of a confined slot jet impingement. The parametric effects of jet Reynolds numbers and jet separation distance on heat transfer characteristics of the heated target surface are explored. With the measurement of jet mean velocity and turbulence intensity distributions at nozzle exit, two jet flow characteristics at nozzle exit, initially at laminar and transitional/turbulent regimes, are classified.

Chen and Modi [8] examined the mass transfer characteristics of a turbulent slot jet impinging normally on a target wall using numerical simulations at the location where the slot jet emerges from the nozzle. A confinement plate is placed parallel to the target plate. The jet fluid is the same as the stagnant fluid into which the jet emerges. The range of Reynolds numbers examined is from 450 to 20 000 with Prandtl or Schmidt numbers from 1 to 2400. The distance of the target plate from the slot jet varies from 2 to 8 times the slot jet width.

Lin et al. [9] measured the mean velocity components, mean flow direction, turbulent intensities and Reynolds' stresses with a split film probe of hot wire anemometer to investigate the flow field generated by two identical jets of air issuing from plane parallel nozzles in a common end wall and mixing with the ambient room air.

Chiriac and Ortega [10] computed the steady and unsteady flow and heat transfer for a confined two-dimensional slot jet impingement on an isothermal plate. The jet Reynolds number was in the range of 250–750 with Prandtl number and jet-to-plate spacing fixed at 0.7 and 5, respectively. They found that at a Reynolds number between 585 and 610, the flow becomes unsteady.

Miller et al. [11] presented the numerical results of spatially developing, three-dimensional jets issued from circular and non-circular nozzles of identical equivalent diameters. Elliptic, rectangular and triangular jets are considered with aspect-ratios of 1:1 and 2:1.

Few researchers have investigated the mass transfer of an unconfined, low-Reynolds-number slot jet, which has become important since many engineering problems deal with the mass transfer of the fluid with low velocities.

In our laboratory, we first built a domestic gas burner system and found that the configurations of the ports

have considerable effects on the combustion efficiency and the emissions. We later constructed a pair of simplified slot burners [12–15] to simulate the interaction between the individual slit burners. The patterns of the jet flames depended strongly on the air/fuel ratio, the slot exit velocity, and the distance between the two burners. We realized that the mass and momentum transfer between these two burners are important factors.

In order to investigate the detailed physics of a slot burner, the focus of this paper is set on the mass and momentum transfer of an unconfined, low-Reynolds-number slot jet. In the future, the analysis can be extended to the interaction of two slot burners with flame and heat transfer. Because of the low velocity, gravity plays an important role in the transfer of mass and momentum. Experimentally, conventional anemometry is not adequate for measuring such a low-velocity flow field, so we concentrated on the measurement of concentration field as well as flow visualization. Instead of measuring the fluid velocity directly, we relied on computation to examine the flow field.

2. Analysis

2.1. Problem description

The schematic diagram of the slot jet system and the calculated domain are shown in Fig. 1(a) and (b), respectively. The slot jet exit is 1 cm wide and 4 cm long, and the width of the wall is about 2 mm. The flow field of a slot jet at low Reynolds numbers ($Re = 39.4$ and 78.8) was examined numerically and experimentally. The slot exit velocities are small, so the gravitational force has to be taken into consideration in numerical calculation. Experimentally, the fluid containing oxygen and nitrogen was issued from a slot jet into the quiescent atmosphere. The concentration field was measured by using a gas chromatograph and a gas-extracting quartz probe. Furthermore, the qualitative aspects of the flow fields were performed by flow visualization obtained with laser-sheet-light illumination of smoke particles.

Oxygen and nitrogen were chosen as the test gases to simulate a two-species mass transfer problem just for experimental convenience. The problem can be extended to a fuel–air application.

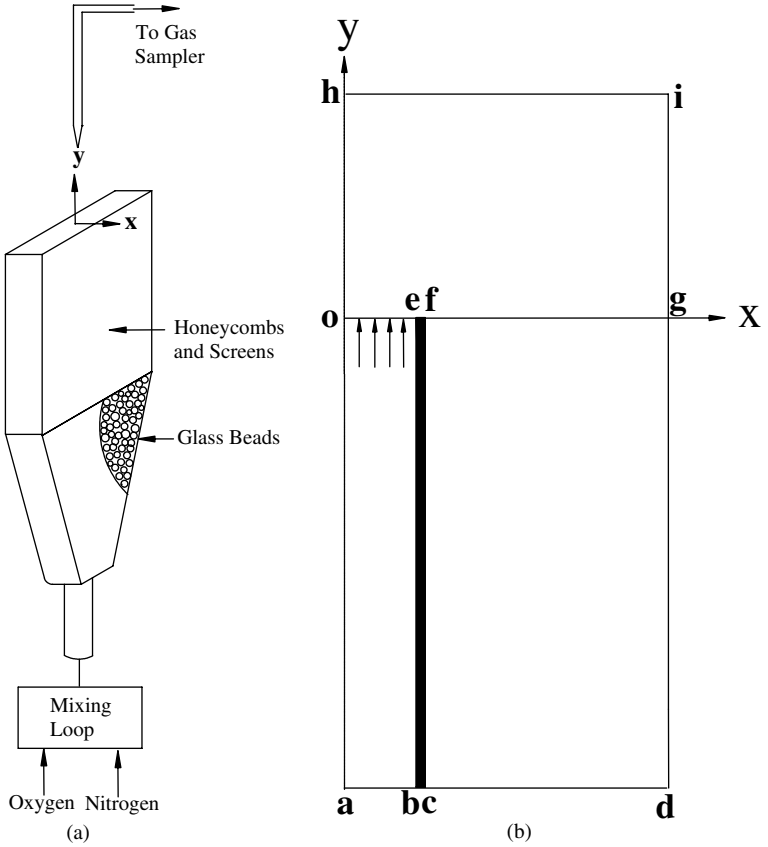

Fig. 1. Schematic diagram of (a) the slot jet system and (b) the calculated domain.

2.2. Numerical analysis

The above slot jet problem was solved numerically based on the following assumptions:

(1) The flow field is steady.
(2) The flow in the third dimension is negligible.
(3) No reaction of the two species is present.
(4) The exit flow at the slot is uniform.
(5) All physical properties of the fluid are based on the room temperature values.
(6) Only oxygen and nitrogen are considered in our analysis, so $Y_{O_2} + Y_{N_2} = 1$.

The slot exit velocity V'_{in} and the slot width b' are employed to non-dimensionalize the governing equations

$$u = \frac{u'}{V'_{in}}, \quad v = \frac{v'}{V'_{in}}, \quad x = \frac{x'}{b'_{in}}, \quad y = \frac{y'}{b'} \tag{1}$$

and

$$P = \frac{P'}{\rho'_{O_2} V'^2_{in}}, \quad Y_{O_2} = \frac{Y_{O_2} - Y_{O_2,\infty}}{Y_{O_2,in} - Y_{O_2,\infty}}, \quad \rho = \frac{\rho'}{\rho'_{O_2}} \tag{2}$$

where $Y_{O_2,\infty}$ is the ambient oxygen concentration.

It should be noted that we define Re^* and Sc^* based on the properties of oxygen instead of the properties of mixture for convenience of programming. It can be shown that the values of the non-dimensional numbers based on oxygen or mixture are within 1% difference. Froude number Fr is defined by conventional parameters.

$$Re^* = \frac{\rho'_{O_2} V'_{in} b'}{\mu'_{O_2}}, \quad Sc^* = \frac{\mu'_{O_2}}{\rho'_{O_2} D'_{O_2-N_2}}, \quad Fr = \frac{V'_{in}}{\sqrt{g' b'}} \tag{3}$$

The four non-dimensionalized governing equations representing the conservations of mass, momentum, and species O_2 are listed in Table 1, where ϕ, Γ_ϕ and S_ϕ are to be substituted into the following equation [16]:

$$\frac{\partial}{\partial x}\left(\rho u\phi - \Gamma_\phi \frac{\partial \phi}{\partial x}\right) + \frac{\partial}{\partial y}\left(\rho v\phi - \Gamma_\phi \frac{\partial \phi}{\partial y}\right) = S_\phi \tag{4}$$

The density of the gas mixture is determined by the ideal gas equation [17]. The viscosity and diffusivity of the gas mixture are evaluated by the formulas of Bird et al. [18] and Reid et al. [19], respectively. It is noted that $\mu_{mix} = \mu'_{mix}/\mu'_{O_2}$ is the ratio of the absolute viscosity of the gas mixture to the absolute viscosity of oxygen.

2.2.1. Domain and boundary conditions

Only one half domain is calculated because the flow field is symmetrical with respect to the centerline of the jet (see Fig. 1(b)). The calculated domain was chosen as a rectangular region of 10 cm in width and 24 cm in length ($\overline{ad} = 10$ cm, $\overline{ah} = 24$ cm). Since the region abeo is the fluid inside the duct and bcfe is the solid wall, these two regions do not need to be calculated and hence we blocked off them ($\overline{ao} = 16$ cm). The corresponding boundary conditions are summarized as follows:

(A) on the symmetrical axis $\overline{oh}$:

$$u = 0, \quad \frac{\partial v}{\partial x} = 0, \quad \frac{\partial Y_{O_2}}{\partial x} = 0 \tag{5}$$

(B) far away from the slot:
(i) at $\overline{hi}$ and $\overline{cd}$

$$\frac{\partial u}{\partial y} = 0, \quad \frac{\partial v}{\partial y} = 0, \quad \frac{\partial Y_{O_2}}{\partial y} = 0 \tag{6}$$

(ii) at $\overline{di}$

$$\frac{\partial u}{\partial x} = 0, \quad \frac{\partial v}{\partial x} = 0, \quad \frac{\partial Y_{O_2}}{\partial x} = 0 \tag{7}$$

(C) slot exit boundary condition $\overline{oe}$:

$$u = 0, \quad v = 1, \quad Y_{O_2} = 1 \tag{8}$$

(D) along the upper solid surface $\overline{ef}$:

$$u = 0, \quad v = 0, \quad \frac{\partial Y_{O_2}}{\partial y} = 0 \tag{9}$$

(E) along the right solid surface $\overline{cf}$:

$$u = 0, \quad v = 0, \quad \frac{\partial Y_{O_2}}{\partial x} = 0 \tag{10}$$

2.2.2. Numerical algorithm

The set of governing equations with boundary conditions were then solved by SIMPLER algorithm with the power-law scheme, and the convergent standard is

Table 1
Governing equations for a slot jet

ϕ	Γ_ϕ	S_ϕ
1	0	0
u	$\frac{\mu_{mix}}{Re^*}$	$-\frac{\partial P}{\partial x} + \frac{1}{3}\frac{\partial}{\partial x}\left(\frac{\mu_{mix}}{Re^*}\frac{\partial u}{\partial x}\right) - \frac{2}{3}\frac{\partial}{\partial x}\left(\frac{\mu_{mix}}{Re^*}\frac{\partial v}{\partial y}\right) + \frac{\partial}{\partial y}\left(\frac{\mu_{mix}}{Re^*}\frac{\partial v}{\partial x}\right)$
v	$\frac{\mu_{mix}}{Re^*}$	$-\frac{\partial P}{\partial y} + \frac{\rho_\infty - \rho}{Fr^2} + \frac{1}{3}\frac{\partial}{\partial y}\left(\frac{\mu_{mix}}{Re^*}\frac{\partial v}{\partial y}\right) - \frac{2}{3}\frac{\partial}{\partial y}\left(\frac{\mu_{mix}}{Re^*}\frac{\partial u}{\partial x}\right) + \frac{\partial}{\partial x}\left(\frac{\mu_{mix}}{Re^*}\frac{\partial u}{\partial y}\right)$
Y_{O_2}	$\frac{\rho}{Re^* Sc^*}$	0

10^{-4}. The grid-independence has been checked in each case. Therefore, the calculated results are all mesh-independent solutions.

2.3. Experimental analysis

2.3.1. Experimental apparatus

Experiments were performed using a 1×4 mm slot jet, as depicted in Fig. 1(a). The wall of the slot jet is 2 mm thick. Several layers of honeycombs and meshed screens were installed inside the jet in order to produce a uniform velocity distribution at the exit plane of the jet. Oxygen and nitrogen were separately controlled by conventional flow meters and pressure gauges, premixed by several mixing loops and then introduced into the slot jet. Therefore, the gases were mixed well to form a uniform mixture. The gaseous mixture of oxygen and nitrogen was issued from a slot jet into the quiescent atmosphere.

2.3.2. Concentration measurements

Shown in Fig. 1(a), the concentration measurements were made by extracting the gas from the flow field by a quartz probe and a vacuum glass bottle with a control valve. A small amount of collected gas was drawn out from the bottle and then injected into the gas chromatograph (GC-14B type, Shimadzu) for analysis on O_2 concentration. The quartz probe was arranged vertically downward when the gas above the slot exit was extracted but was arranged upward when the gas below the slot exit was extracted hence the flow field was free from interference of the quartz probe. The quartz probe has a very small tip opening (approximately 0.1 mm inside diameter) and its extraction speed is small enough to ensure that the gas extraction is confined in a small neighboring region of a fixed point. The tip of the quartz probe can be traversed both horizontally and vertically by means of a three-dimensional positioner.

2.3.3. Flow visualization

Smoke particles were used to visualize the low-velocity flow fields because the flow cannot carry heavy particles due to small initial momentum at the slot exit. The smoke particles were injected into the flow and mixed well with the fluid and then issued from the slot exit. A thin sheet of laser light, about 1 mm thick, is used to shine on the particles to make the flow visible [20]. A video camera was used to take the photographs continuously.

3. Results and discussions

Two different exit oxygen concentrations ($Y_{O_2,in} = 0.21, 0.5$) corresponding to two exit velocities were discussed here to illustrate the effect of mass and momentum transfer.

For the purpose of comparison, we first computed flow fields with no mass diffusion. Fig. 2(a) shows the calculated velocity fields for slot exit oxygen concentration $Y_{O_2,in} = 0.21$ with exit velocity $V'_{in} = 0.06$ m/s. The corresponding Reynolds numbers, Schmidt numbers and Froude numbers are respectively 39.4, 0.743 and 0.192. The fluid decelerates in the y-direction due to

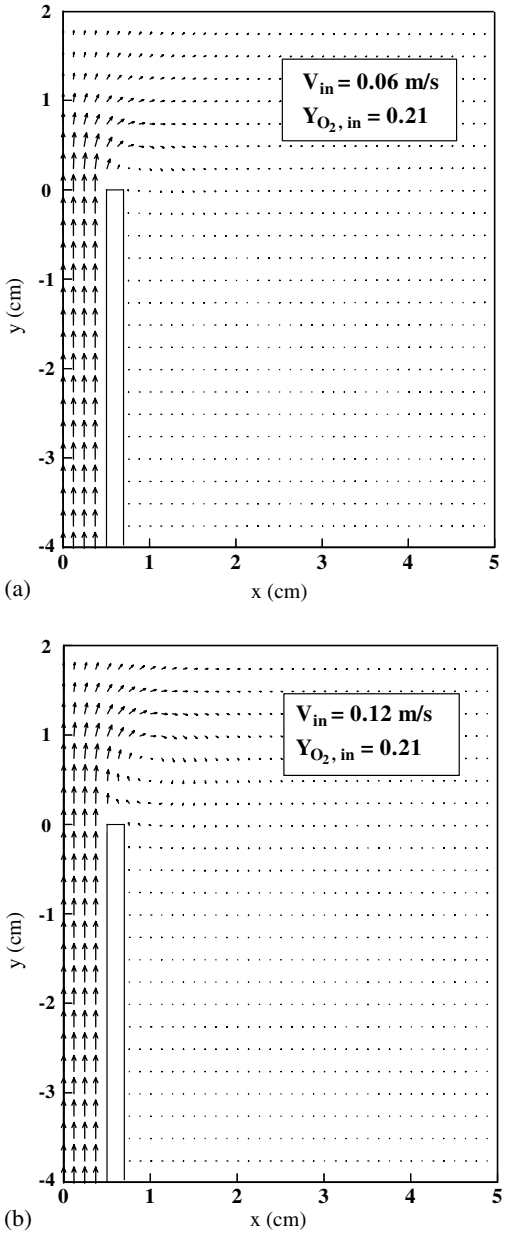

Fig. 2. The calculated velocity field for slot exit oxygen concentration 0.21 and slot exit velocity (a) 0.06 m/s (b) 0.12 m/s.

the viscous stress between the moving fluid and the quiescent atmosphere. Because the momentum of the fluid at the slot exit is very small, the fluid expands immediately. Because the density of the mixture is equal to the air density, so the buoyancy effect can be excluded. As the slot exit velocity increases to $V'_{in} = 0.12$ m/s (Fig. 2(b)), the initial momentum is greater than the case for $V'_{in} = 0.06$ m/s. A small amount of air is entrained and then mixes with the moving fluid to form a recirculation vortex. For the case of $Y_{O_2,in} = 0.21$, no mass diffusion was present, only momentum transfer is important in this kind of flow field.

The velocities and concentration fields for slot exit oxygen concentration $Y_{O_2,in} = 0.5$ (with a considerable mass transfer) corresponding to the same slot exit velocities will be illustrated in Figs. 3–12.

Fig. 3 shows the calculated velocity and concentration fields for slot exit velocity $V'_{in} = 0.06$ m/s and slot exit oxygen concentration $Y_{O_2,in} = 0.5$. Since the momentum of the fluid at the slot exit is very small and the density of the mixture is larger than the air density, only a small part of the fluid moves along the original flow direction (upward). Most of the fluid turns downwards and air is entrained from the upper and upper-right regions. A vortex occurs (the center of the vortex is located at about $x = 2.7$ cm and $y = -1.2$ cm) far away from the slot exit due to the air entrainment and the shear force between the moving fluid and the quiescent fluid.The merged flow continues to move downwards and mixes with air, so the O_2 concentration becomes smaller and smaller. Gravitational force plays an important role, especially in the regions where the inertia force is comparatively small. The vortex near the slot exit region was not apparent for such small exit velocity.

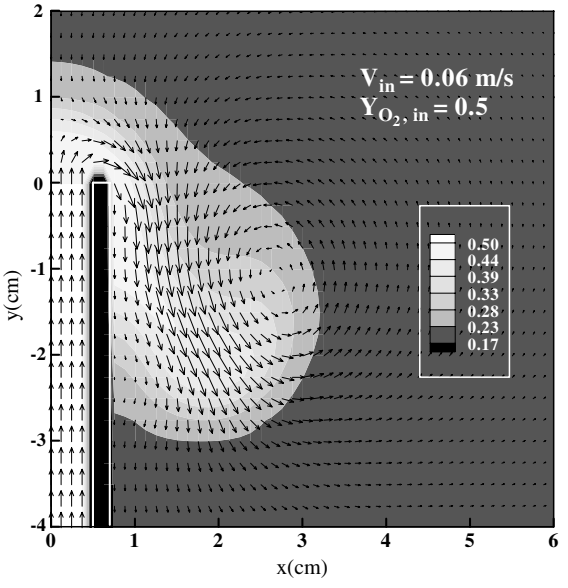

Fig. 3. The calculated velocity field and concentration field for slot exit velocity 0.06 m/s and slot exit oxygen concentration 0.5.

Fig. 4 shows the experimental and calculated concentration contours of O_2. We can see the O_2 concentration is 0.5 at the slot exit and then decreases gradually until the atmosphere value 0.21 due to momentum and mass transfer. It takes about 1.3 cm for the O_2 concentration to decay to 0.21 in upward direction, but about 2 cm to the right side of the jet wall. We can further see that the experimental and numerical results coincide in the region above the slot exit but are moderately different in the region below the slot exit.

Fig. 5 shows the transverse concentration distributions at different longitudinal positions. Three cross-sections of the contour map are selected to compare the numerical and experimental results. The computed results show that the O_2 concentrations decay smoothly and monotonously in x-direction for different y. For $y = 0.2$ cm, the O_2 concentration is 0.5 at $x = 0$ cm and then decays to about 0.39 at $x = 1$ cm, and then decays to the atmosphere value at $x = 3.0$ cm. The experimental result shows that the O_2 concentration is lower than the numerical result at $x < 0.9$ cm and higher than the numerical result at $x \geqslant 0.9$ cm. For $y = 0.6$ cm, the calculated O_2 concentration is 0.45 at $x = 0$ cm and then decays to about 0.27 at $x = 1$ cm, and then decays to 0.21 at $x = 2.6$ cm. The experimental result is in good agreement with the numerical result except for the region 1.0 cm $< x <$ 1.8 cm. For $y = 1.0$ cm, the O_2 concentration is 0.27 at $x = 0$ cm and then decays to about 0.235 at $x = 1$ cm, and then decays to 0.21 at $x = 2.2$ cm. We find the region of mass transfer for experiment larger than for calculation.

Fig. 6 shows the longitudinal distributions of the O_2 concentrations at different transverse positions. Three cross-sections ($x = 0$, 0.4, and 0.8 cm) are selected to compare the numerical and experimental results. At the centerline ($x = 0$ cm), the O_2 concentration is 0.5 at slot exit ($y = 0$ cm) and then decays smoothly and rapidly along y-direction until it reaches 0.28 at $y = 1$ cm, and then reaches 0.21 at $y = 2.4$ cm. For $x = 0.4$ cm, which is located at the inside wall of the slot, the O_2 concentration decays to 0.26 at $y = 1$ cm and 0.21 at $y = 2.1$ cm. For $x = 0.8$ cm, which is located outside the wall and above the jet exit, the O_2 concentration distribution is almost the same as $x = 0.4$ cm. Further observation indicates that the concentration decays more quickly in y-direction than in x-direction.

Fig. 7 shows the photograph of the flow visualization and the calculated velocity field for the slot exit velocity $V'_{in} = 0.06$ m/s. These two flow fields are similar in qualitative sense. The numerical results have been discussed in Fig. 3. For flow visualization, the distance that the fluid can reach is about 0.8 cm in upward direction,

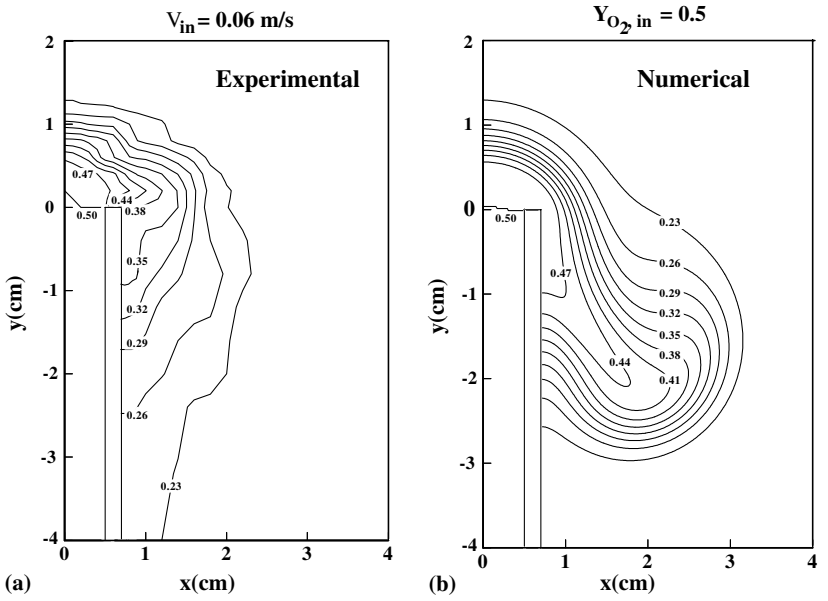

Fig. 4. Concentration contours for slot exit velocity 0.06 m/s and slot exit oxygen concentration 0.5 (a) experimental and (b) numerical results.

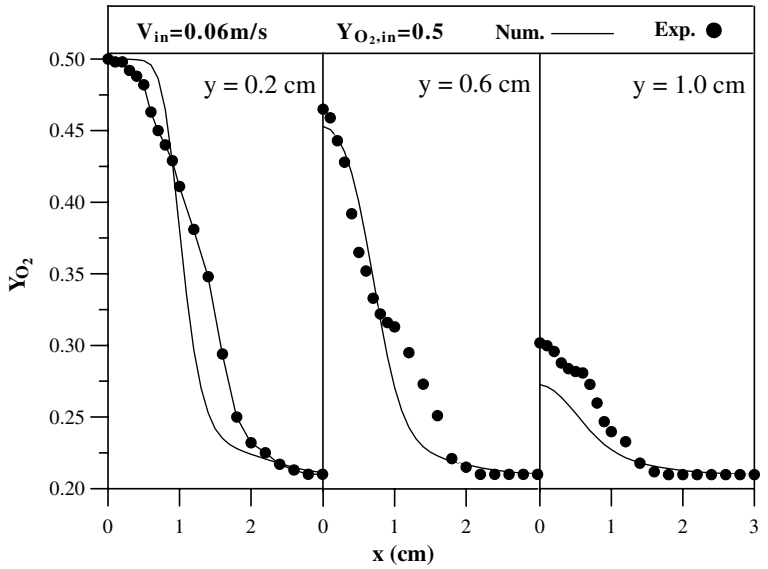

Fig. 5. Transverse concentration distributions at different longitudinal positions for slot exit velocity 0.06 m/s and slot exit concentration 0.5.

and the vortex is located at about $x = 2.7$ cm and $y = -2.2$ cm. It appears that the distances in upward and right region that the fluid can reach are almost the same. The x coordinate of the center of the vortex for the experiment is the same with the calculated result, but the y coordinate is about 1.0 cm lower than the calculated result. The smoke particles may have slightly affected the diffusion, and perhaps did not follow the flow completely.

Fig. 8 shows the calculated velocity and O_2 concentration fields for slot exit velocity $V'_{in} = 0.12$ m/s with exit oxygen concentration $Y_{O_2,in} = 0.5$. The corresponding Reynolds numbers, Schmidt numbers and Froude numbers are respectively 78.8, 0.743, and 0.383. We can

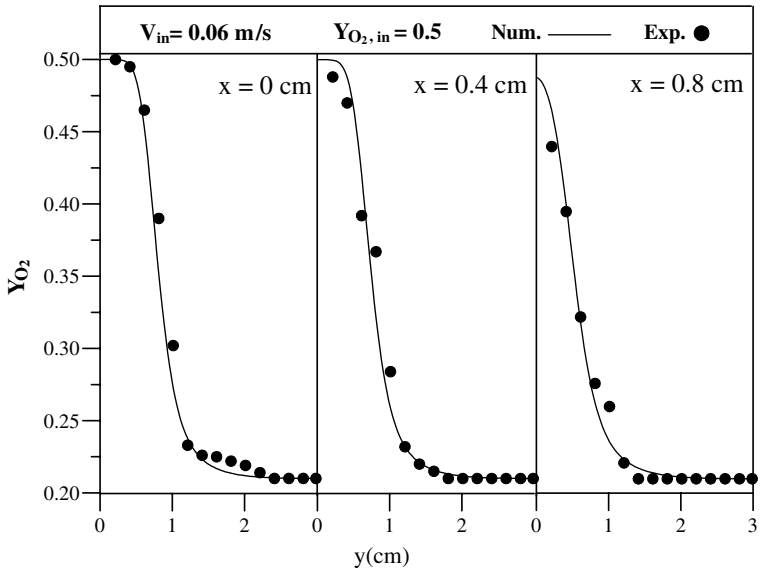

Fig. 6. Longitudinal concentration distributions at different Transverse positions for slot exit velocity 0.06 m/s and slot exit concentration 0.5.

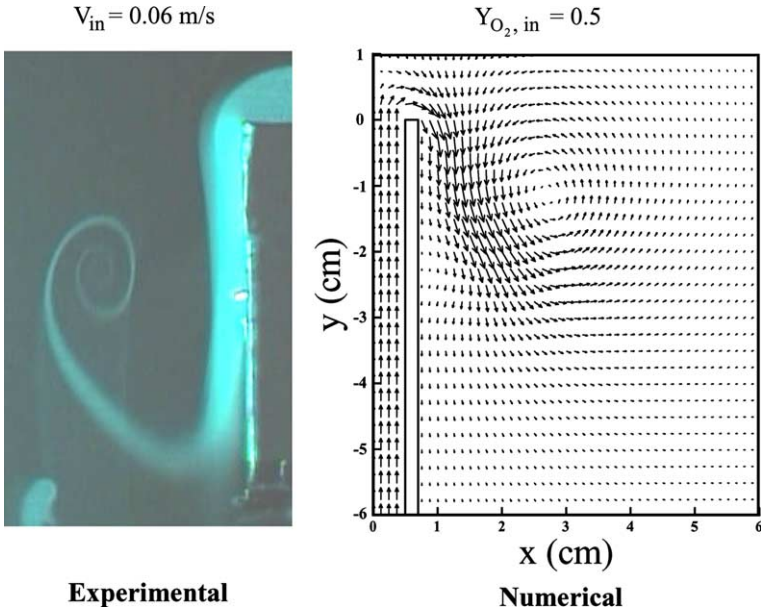

Fig. 7. The flow visualization and the calculated velocity field for slot exit velocity 0.06 m/s and slot exit oxygen concentration 0.5.

see the fluid moves farther away from the slot exit in the y-direction along the centerline than in the former case ($V'_{in} = 0.06$ m/s) due to larger initial momentum. The initial momentum brings the fluid away from the slot exit in y-direction, but the gravitational force pulls back the fluid, so the fluid turns down at a distance from the slot exit. A recirculation vortex near the slot exit whose vortex center is located at about $x = 0.9$ cm and $y = 0.4$ cm can be seen. A small amount of the down-flowing fluid turns inwards and impinges on the solid wall and then turns outwards. Another vortex due to shear force far away from the slot exit (the center of the vortex is located at about $x = 2.5$ cm and $y = -0.3$ cm) can also be seen. The concentration field depends strongly on the velocities since the momentum transfer dominates most part of the flow field.

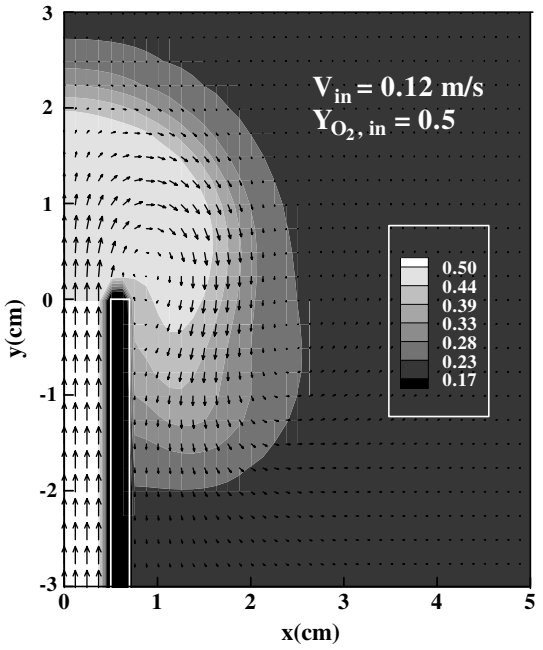

Fig. 8. The calculated velocity field and concentration field for slot exit velocity 0.12 m/s and slot exit oxygen concentration 0.5.

Fig. 9 shows the experimental and calculated concentration contours of O_2. We can see the distance that O_2 can reach is about 2.2 cm in y-direction above the slot exit, and is about 2.5 cm in x-direction. The diffusion distance for O_2 in y-direction is apparent larger than for the case of $V'_{in} = 0.06$ m/s. Furthermore, the calculated and experimental results are in fairly good agreement, but larger difference exists in the right-lower region.

It is interesting to note that saddle-shaped concentration distributions can be seen at longitudinal positions $y = 0.2$, 0.6 and 1.0 cm (see Fig. 10). It is due to the appearance of recirculation vortex in the near field region of the slot exit. We first discuss the numerical results. For $y = 0.2$ cm, the O_2 concentration is exactly 0.5 at $x = 0$ cm, and has a local minimum value 0.44 (at $x = 0.7$ cm). The O_2 concentration then increases to 0.47 (at $x = 1.2$ cm), and then decay monotonously till 0.21 (at about $x = 3.0$ cm). For $y = 0.6$ cm, the curve is qualitatively similar to that at $y = 0.2$ cm, but the concentration peak and valley are not as apparent as those at $y = 0.2$ cm. For $y = 1.0$ cm, the concentration peak and valley almost disappear since $y = 1.0$ cm is near the rim region of the vortex. The saddle-shaped curve will disappear far away from the vortex. Experimentally, the results agree qualitatively with the numerical results. Quantitatively, the experimental results decay more quickly in most part of the region partly because the fluid flows out of the short end of the slot, which can be attributed to the three-dimensional effects.

From Fig. 11, we can see the O_2 concentration on the centerline ($x = 0$ cm) decays more slowly than that for $V'_{in} = 0.06$ m/s. The calculated results agree with the experimental results in qualitative sense. Quantitatively, the experimental results decay more quickly due to the three-dimensional effect.

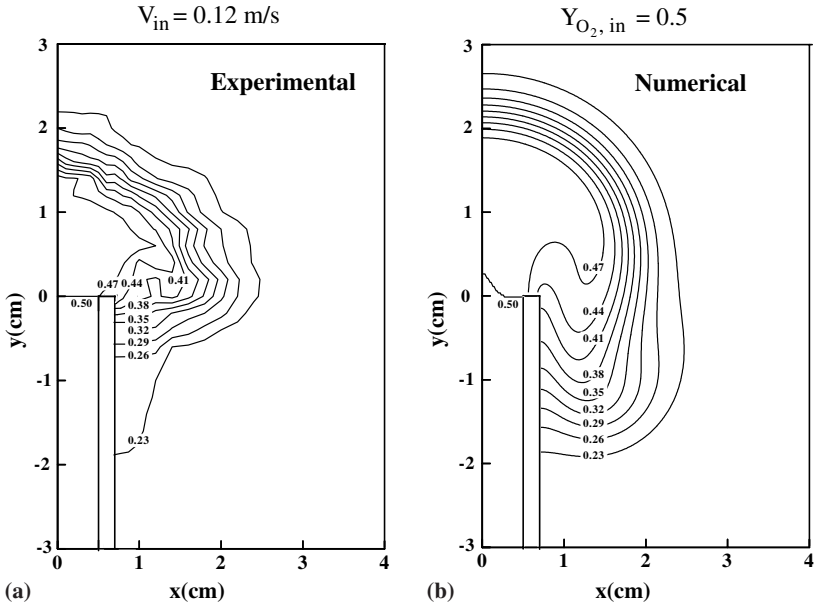

Fig. 9. Concentration contours for slot exit velocity 0.12 m/s and slot exit oxygen concentration 0.5 (a) experimental and (b) numerical results.

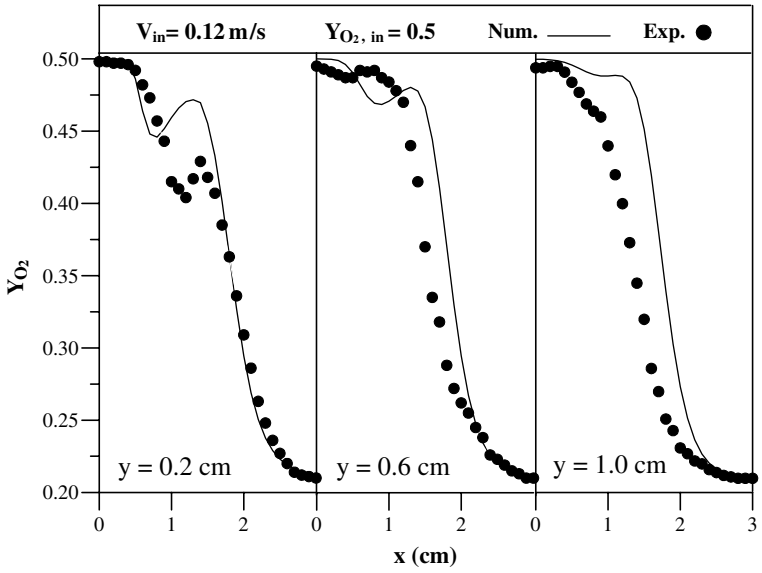

Fig. 10. Transverse concentration distributions at different longitudinal positions for slot exit velocity 0.12 m/s and slot exit concentration 0.5.

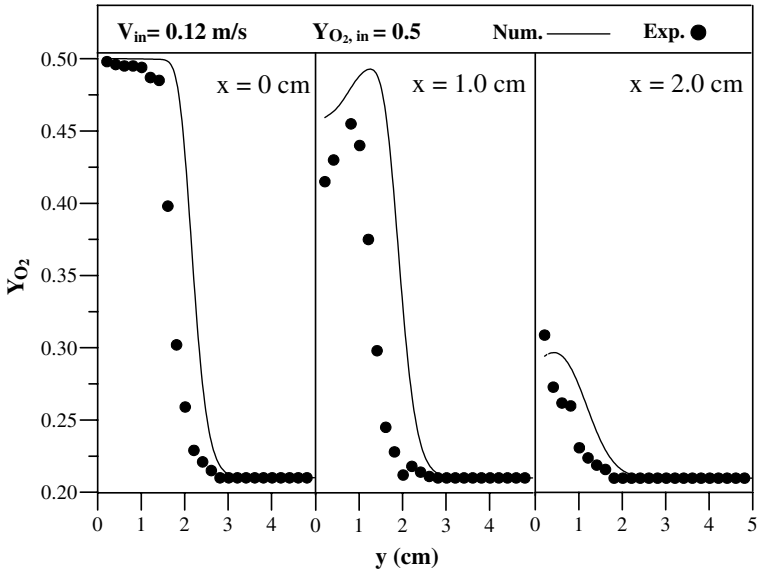

Fig. 11. Longitudinal concentration distributions at different transverse positions for slot exit velocity 0.12 m/s and slot exit concentration 0.5.

Fig. 12 shows the photograph of the flow visualization and the calculated velocity field for the slot exit velocity $V'_{in} = 0.12$ m/s. We can see the length needed to turn-down for the computation is slightly smaller than that of the experiment, hence, the size of the corresponding vortex in the computation is also smaller than of the experiment. The vortex outside the main flow can be seen for computations, but not in the experiments. It is possibly because the smoke particles do not follow the gas flow in some local region.

In all the above-mentioned cases, the gravitational force has been downwards because the density of the jet is larger than the atmospheric air. If the gravitational force is reversed in direction by introducing a lighter jet into the atmosphere, the velocity and concentration field can considerably be changed. Fig. 13(a) and (b) show

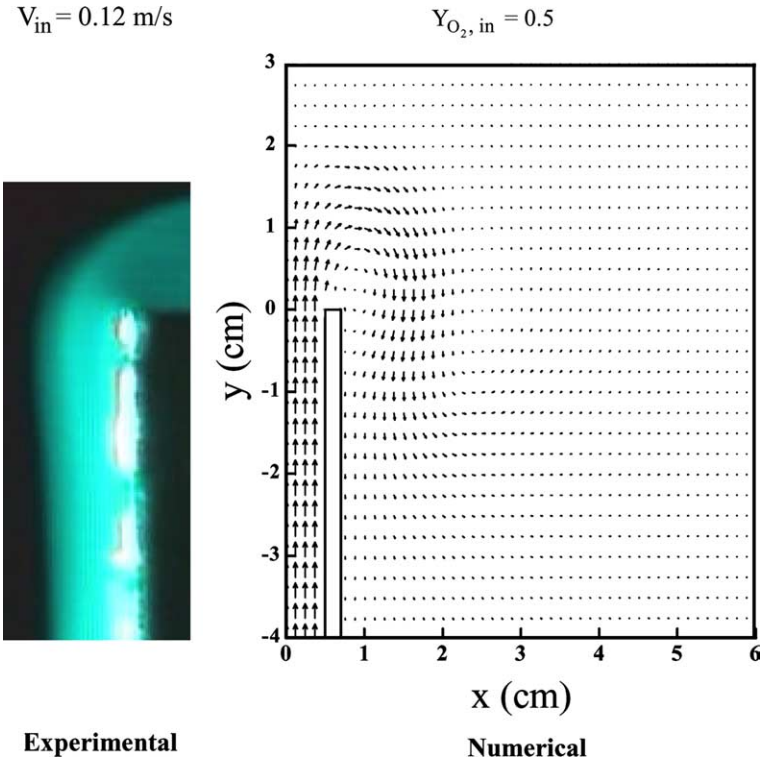

Fig. 12. The flow visualization and the calculated velocity field for slot exit velocity 0.12 m/s and slot exit oxygen concentration 0.5.

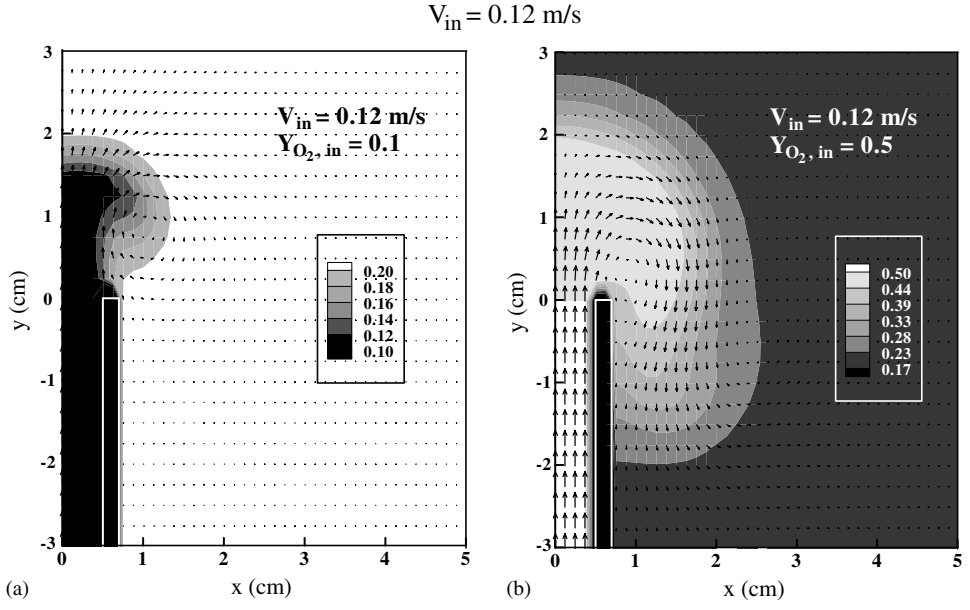

Fig. 13. The comparison between the results of slot exit oxygen concentration (a) 0.1 and (b) 0.5 for slot exit velocity 0.12 m/s.

two jets at the same exit velocity, $V'_{in} = 0.12$ m/s, but at two different mole fractions of $Y_{O_2,in} = 0.1$ and 0.5. Fig. 13(b) is the same as Fig. 8, and has been discussed earlier in the text. Because the density for $Y_{O_2,in} = 0.1$ is smaller than the air, the buoyancy term, $(\frac{\rho_\infty - \rho}{Fr^2})$ in the governing equations changes its sign. Due to the contribution of

the buoyancy term, more fluid moves upwards than the case for $Y_{O_2,in} = 0.5$, so the position of the vortex center for $Y_{O_2,in} = 0.1$ ($x = 0.95$ cm and $y = 0.85$ cm) is higher than for $Y_{O_2,in} = 0.5$ ($x = 0.9$ cm and $y = 0.4$ cm). Further observation can be made that the mass-diffusion distances for these two cases do not differ much in upward direction but larger difference exists in the right-lower region. The saddle-shaped concentration curve cannot be seen for $Y_{O_2,in} = 0.1$ because the fluid was not pulled downwards by the gravitational force.

4. Conclusions

The velocity and concentration fields of a slot jet at low Reynolds numbers were numerically computed, and the computed results were compared with experimentally obtained concentration field and flow visualization. The Reynolds number (the ratio of inertia to viscous forces) and Schmidt number (the ratio of the momentum to mass diffusivities) is not sufficient to characterize this kind of unconfined binary-mixture slot jet flow field. In addition to the Reynolds number and the Schmidt number, the Froude number, defined as $Fr = \frac{V'_{in}}{\sqrt{g'b'}}$ (the ratio of inertial forces to gravity forces), is also important. In the present study, two apparently different flow fields corresponds to $Fr = 0.192$ and 0.383 (i.e. $V'_{in} = 0.06$ and 0.12 m/s) were used to illustrate the effect of Froude number. Since the Froude number is smaller than 1.0, the gravitational force has to be taken into consideration. It was found that the fluid was strongly influenced by the gravitational force in the case of $V'_{in} = 0.06$ m/s but was moderately influenced by the gravitational force in the case of $V'_{in} = 0.12$ m/s.

The conclusions are as follows:

(1) The flow and concentration fields are characterized by the strong interaction among momentum transfer, mass transfer and gravitational force.
(2) For high-density jet discharging upwards into quiescent air, the gravitational force acts to accelerate the fluid in the downward direction. At $Re = 39.4$, one vortex in the far region exists. The distance that O_2 can reach is about 1.3 times the slot width in y-direction above the slot exit, and is about 2.0 times the slot width in x-direction.
(3) At $Re = 78.8$, two vortices appear; one attached at the slot exit and one in the far region. The distance that O_2 can reach is about 2.2 times the slot width in y-direction above the slot exit, and is about 2.5 times the slot width in x-direction.
(4) The calculated results are in fairly good agreement with the experimental results; therefore, the numerical model was found to represent a low-Reynolds-number slot jet adequately and can be used to relieve some experimentation difficulties.

Acknowledgements

This study was supported by National Science Council, Taiwan, ROC under the contracts of NSC 89-2212-E-168-003 and NSC90-2212-E-006-083.

References

[1] E.C. Panzer, D.P. Telionis, On the spreading of slotted jets, Exp. Thermal Fluid Sci. 18 (1988) 210–219.
[2] E. Baydar, Confined impinging air jet at low Reynolds numbers, Exp. Thermal Fluid Sci. 19 (1999) 27–33.
[3] F.G. Roper, C. Smith, A.C. Cunningham, The prediction of laminar jet diffusion flame sizes: part II: experimental verification, Combust. Flame 29 (1997) 227–234.
[4] T. Yuan, D. Durox, E. Villermaux, An analogue study for flame flickering, Exp. Fluids 17 (1994) 337–349.
[5] M. Amielh, T. Djeridane, F. Anselmet, L. Fulachier, Velocity near-field of variable density turbulent jets, Int. J. Heat Mass Transfer 39 (1996) 2149–2164.
[6] R.M.M. Mallens, H.C. de Lange, C.H.J. Van de Ven, L.P.H. de Geoy, Modeling of confined and unconfined laminar premixed flames on slit and tube burners, Combust. Sci. Technol. 107 (1995) 387–401.
[7] Z.H. Lin, Y.J. Chou, Y.H. Hung, Heat transfer behaviors of a confined slot jet impingement, Int. J. Heat Mass Transfer 40 (1997) 1095–1107.
[8] Q. Chen, V. Modi, Mass transfer in turbulent impinging slot jets, Int. J. Heat Mass Transfer 42 (1998) 873–887.
[9] Y.F. Lin, M.J. Sheu, Investigation of two plane parallel unventilated jets, Exp. Fluid 10 (1990) 17–22.
[10] V.A. Chiriac, A. Ortega, A numerical study of the unsteady flow and heat transfer in a transitional confined slot jet impinging on an isothermal surface, Int. J. Heat Mass Transfer 45 (2002) 1237–1248.
[11] R.S. Miller, C.K. Madnia, P. Givi, Numerical simulation of non-circular jets, Comput. Fluids 24 (1995) 1–25.
[12] Y.C. Ko, S.S. Hou, T.H. Lin, Combustion characteristics of a single gas-stove with various burner orientation, in: National Conference on Combustion Science and Technology, Tainan, Taiwan, ROC, 1998, pp. 309–314 (in Chinese).
[13] J.C. Sheu, G.T. Lin, R.H. Chen, T.H. Lin, Concentration distributions of two interacting laminar diffusion flames, in: National Conference on Combustion Science and Technology, Taoyuan, Taiwan, ROC, 1996, pp. 107–112 (in Chinese).
[14] I.C. Wang, S.S. Hou, T.H. Lin, Buoyancy effects on flickering jet-flames, in: National Conference on Combustion Science and Technology, Kaohsiung, Taiwan, ROC, 2002, pp. 229–236 (in Chinese).
[15] I.C. Wang, S.S. Hou, T.H. Lin, Step effects on interacting jet flames, in: National Conference on Combustion Science and Technology, Kaohsiung, Taiwan, ROC, 2002, pp. 237–244 (in Chinese).
[16] S.V. Patankar, Numerical Heat Transfer and Fluid Flow, Hemisphere, New York, 1980, pp. 80.

[17] S.S. Hou, K.C. Chang, T.H. Lin, Analysis of finite laminar opposed-jets with and without rigid-body rotation, Int. J. Heat Mass Transfer 35 (1992) 945–956.
[18] R.B. Bird, W.E. Stewart, E.N. Lightfoot, Transport Phenomena, Wiley, New York, 1960, pp. 24–25.
[19] R.C. Reid, J.M. Prausnitz, T.K. Sherwood, The Properties of Gases and Liquids, McGraw-Hill, New York, 1997.
[20] S.S. Hou, T.H. Lin, A liquid-pool simulation on droplet combustion in a swirl flow, ASME J. Energy Resour. Technol. 117 (1993) 175–182.